Advances in Science and Technology Research Journal

Advances in Science and Technology Research Journal, 2025, 19(3), 27–36
https://doi.org/10.12913/22998624/197034
ISSN 2299-8624, License CC-BY 4.0

Received: 2024.11.11
Accepted: 2025.01.10
Published: 2025.02.01

Surface reconstruction and dimensional accuracy calculations of cranial implant for biomedical engineering

Ali Mohammed Jassem Al-Bdairy[1]

[1] Production Engineering and Metallurgy Departament, University of Technology, Baghdad, Iraq
E-mail: ali.m.jassem@uotechnology.edu.iq

ABSTRACT

Designing accurate cranial implants of a specific patient is a time-consuming procedure for designing and manufacturing; hence, in the present work, a full and fast procedure for designing and manufacturing a cranial implant was carried out. On the basis of biomedical engineering data, the damaged zone was detected as boundary intersection, a special algorithm for surface reconstruction was adopted, rather than repairing the damaged members/zone based on additive manufacturing technology. Fixation parts and porosity were designed to fix the implant with the skull, and decrease the overall weight of the designed implant, respectively. The difference between defective skull and the designed cranial implant was achieved based on the image processing technique. The obtained difference value was ranged ±1.861984 mm, where the overall dimension of the studied skull was 205.7, 149.0, 154.9 mm, and the dimensions of the designed cranial implant were 139, 131.1, 38.8 mm.

Keywords: biomedical engineering, cranial implants, image processing, defected skull.

INTRODUCTION

Due to accidents or congenital malformations, some body areas may suffer loss or damage. Skull defects are a common clinical issue, and treating them remains a significant challenge. Currently, no artificial implants or prosthetics can perfectly match and integrate with the growing human skull. Surgical procedures typically involve implanting materials into the damaged area. However, creating accurate cranial implants tailored to individual patients is time-consuming. Fabrication of defected zone in human body or bone has expanded incredible responsiveness in recent years, because the low cost and high accuracy of 3D printing technique made it possible for biomedical engineering applications [1]. 3D printing is a dominant technology that deals with several possible assistances to biomedical engineering, especially in the field of tissue engineering and 3D printing of scaffolds [2]. Contemporary growths of biocompatible materials have assisted in improving 3D bio-printing for regenerative medicine [3]. Some researchers devoted attention to studying the accident losses of human body with prosthetics members or implants. Dong et al. reviewed bioprinting approaches during three phases: pre-processing, processing, and post-processing, which related to improving the quality life of the patients, reducing healthcare costs, and tapping into the global medical device market [4]. Boretti reported on the application of 3D printing in the medical field, such as primarily bioprinting models in surgery preparation, surgical instruments, prosthetics, drugs, drug delivery systems, streamlined drug development process, and educational medical models [5]. Ananth and Jayram summarized the use of the 3D biomaterial scaffolds in bone tissue engineering applications, and the customized application of 3D printing technique in tissue engineering, prostheses, implants, and drug delivery devices [6]. Vindokurov et al. presented an experimental and analytic study of biocompatible polylactic acid (PLA) based on compressive mechanical properties,

especially elastic modulus and ultimate compression strength [7].

Zhang et al. suggested an integrated study for treating the skull defect of children with fast growth of skulls. They also compared the porous polyetheretherketone (PEEK) implant with the non-porous PEEK, cell adhesion, regenerate skull tissues, and the side effects with surrounding tissues among 6 months [8]. Resmi et al., proposed an approach based on 3D U-Net and Transformers to complete the skull shape automatically, and the authors used a vision transformer for the volumetric reconstruction of a skull [9]. In the present work, a methodology for reconstruction of cranial implants of defected skull was presented. This methodology involves a sequential stage of design, fixtures design, dimensional accuracy calculations, and surface reconstruction of a cranial implant.

METHODOLOGY

Modeling a cranial implant was accomplished in several sequential stages, these included; reconstructing the 3D skull model using medical data, and applying engineering modeling concepts to the design of the cranial implant. The adopted methodology procedure is shown in Figure 1.

Design of the cranial implant

A 3D model of the skull was reconstructed using the medical data obtained from imaging devices, such as magnetic resonance imaging (MRI) and computed tomography (CT), which provide digital images of the patient being examined. In this study, medical data from patients in NRRD format was converted into a computerized model using the 3D processing software, 3D Slicer. These models were then exported as 3D STL files or image data in JPG or BMP formats for the subsequent design stages. Figure 2 illustrates the medical data processing conducted with the 3D Slicer software.

It is important to detecting the boundary area of the implant at the beginning of designing the cranial implants for patient skull. Figure 3 present this bounded area of implant patch, which were detected using the MeshMixer software.

The bounded area of the affected side was reflected on the unaffected side, as shown in Figure 3b, to make the intersection situation of

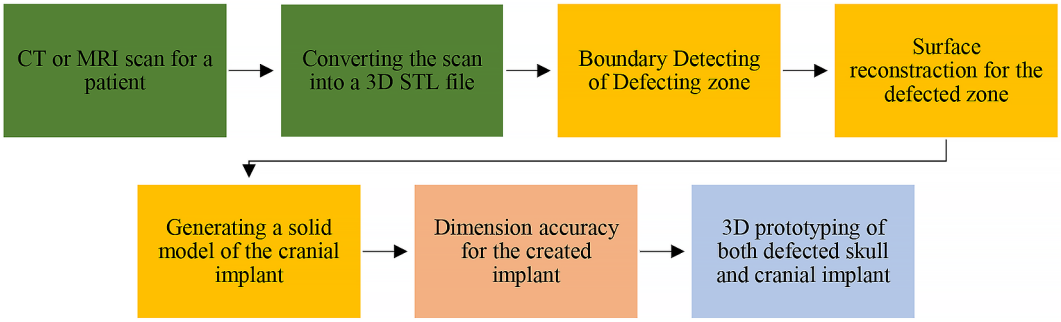

Figure 1. The adopted methodology procedure

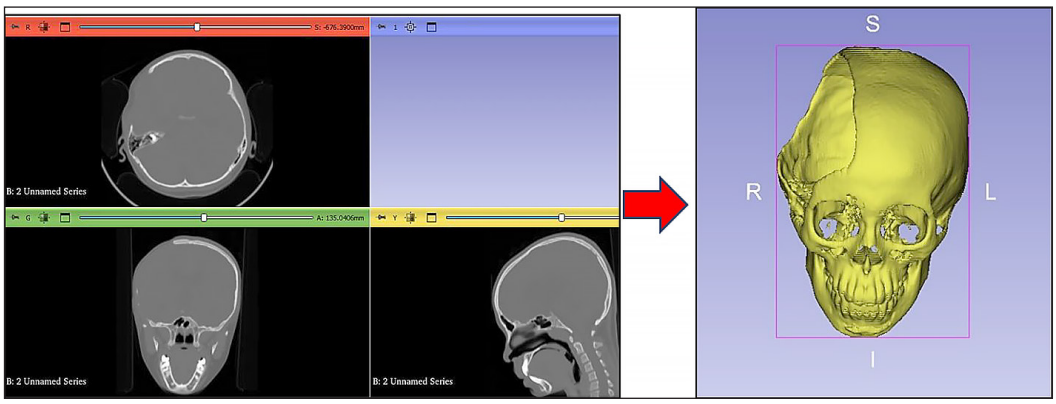

Figure 2. Converting a medical data scan into 3D STL file

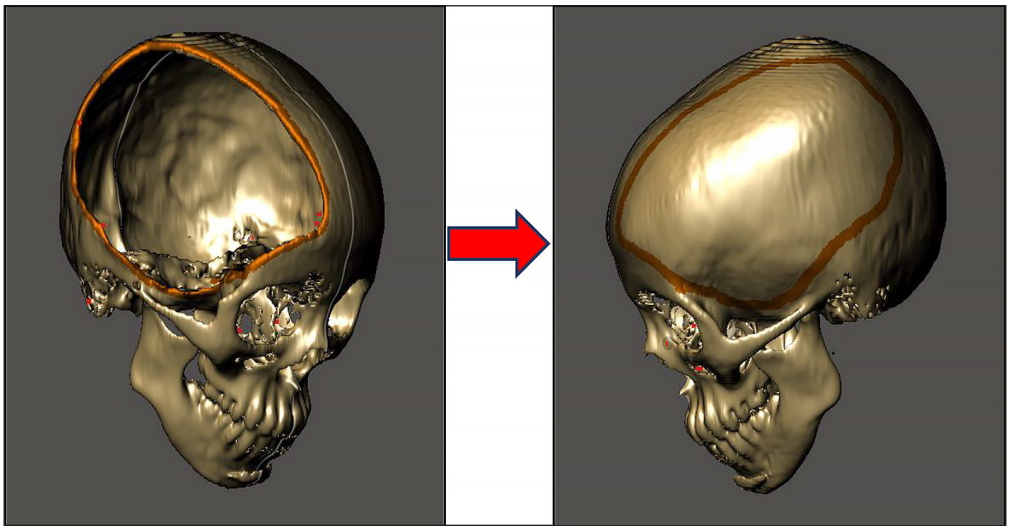

Figure 3. Detecting the cranial implant area

the implant area with the unaffected side of the skull, that based on the intersection equation of the bounded area (rational parametric curve) with skull (rational parametric surface), which is defined as [10];

$$r=r1=\left(\frac{X1(t)}{W_1(t)},\frac{Y1(t)}{W_1(t)},\frac{Z1(t)}{W_1(t)}\right)^T \cap$$

$$r = r2 = \left(\frac{X2(u,v)}{W_2(u,v)},\frac{Y2(u,v)}{W_2(u,v)},\frac{Y2(u,v)}{W_2(u,v)}\right)^T, \quad (1)$$

$$0 \le t,u,v \le 1$$

In this way, the implant patch was generated on the unaffected side, and reflected on the affected zone as a shell model, as shown in Figure 4.

After generation, the implant patch as a shell section in (X,Y,Z) coordinates with two parameters (u) and (v), can reflect the designed shell implant model on the affected side using the reflection (mirror) concept about y,z plan, using the Equation 2 [11,12].

$$\begin{bmatrix} X(u,v)^* \\ Y(u,v)^* \\ Z(u,v)^* \end{bmatrix} = \begin{bmatrix} -1 & 0 & 0 \\ 0 & 1 & 0 \\ 0 & 0 & 1 \end{bmatrix} \cdot \begin{bmatrix} X(u,v) \\ Y(u,v) \\ Z(u,v) \end{bmatrix} \quad (2)$$

Also, it can generate a solid model of cranial implant using the concept of swept surfaces for space curve C(t) notice as the profile along the transformation path may include translation or rotation. The following equation expressed the swept surfaces [13].

$$P(t,w) = C(t) \cdot T(w), 0 \le (t,w) \le 1 \quad (3)$$

Figure 5 presented the designed 3D cranial implants for the affected side of the patient skull. The overall dimension of skull was (205.7, 149.0, 154.9) mm, and the dimension of the designed cranial implant was (139, 131.1, 38.8) mm.

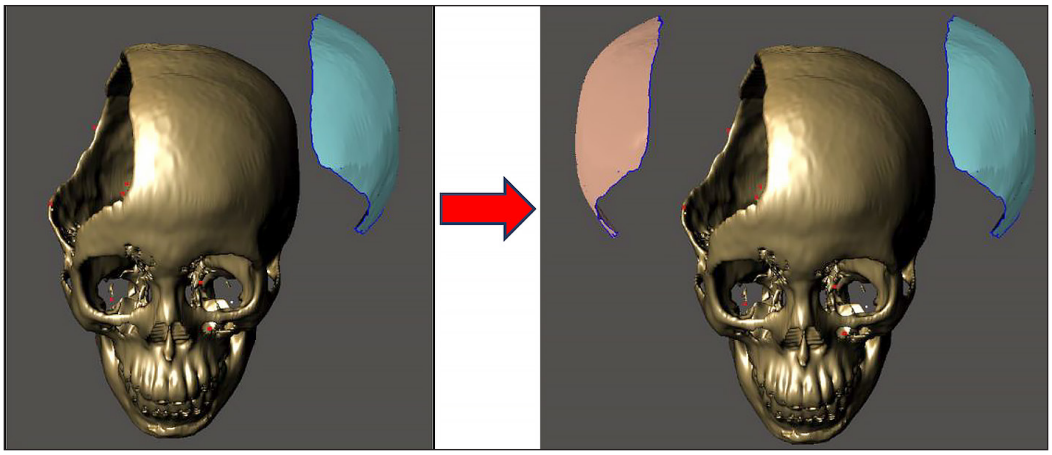

Figure 4. The designed shell model of the cranial implant

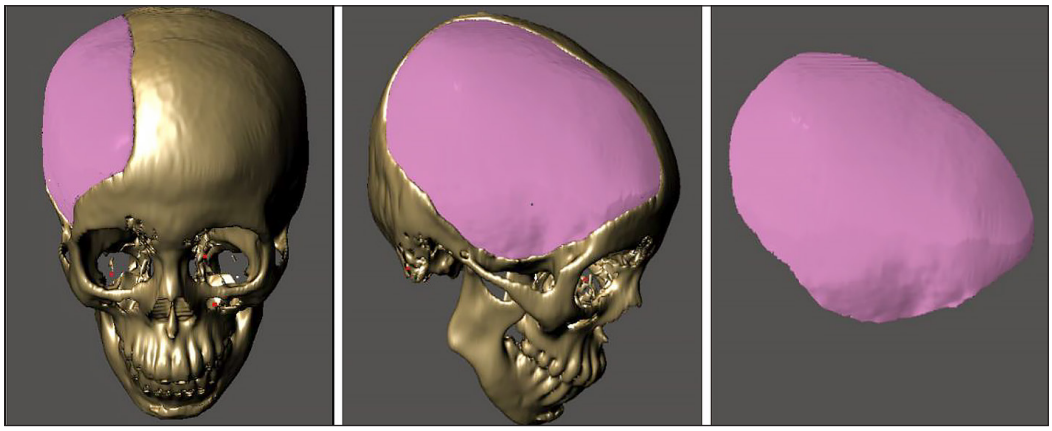

Figure 5. The defected skull and the designed cranial implant for the patient

Fixation design

After designing the cranial implant, fixation parts to fix the implant to the skull. Had to be designed The position and geometry of fixture parts were designed with the dimensions shown in Figure 6. These fixtures were embodied with cranial implant, and it can be mounted using a screw with 2 mm diameter. Also, porosity has been designed with uniform distribution of circular hole with a diameter of 2 mm, to decrease the weight of the overall designed implant. The final shape of the designed cranial implant with fixtures is presented in Figure 7.

Dimensional accuracy of the designed model

The designed cranial implant must have the exact dimension of the defected patch in the skull. Thus, a validation process was executed using the image processing technique. Figure 8 introduced the adopted procedure for dimension accuracy using the Matlab software.

The adopted image processing technique

In the present work, the Matlab software was used to achieve the procedure of image processing technique for dimension accuracy domain. The procedure starting with capturing of multi-views of the cranial implant, and the defected zone of skull for the patient. After that these images were prepared in Matlab and then converted from RGB image into gray scale image; also, visualization enhancement was done. Figure 9 presents the image processing for both cranial implant and the defected zone in the skull of the patient with multiple views.

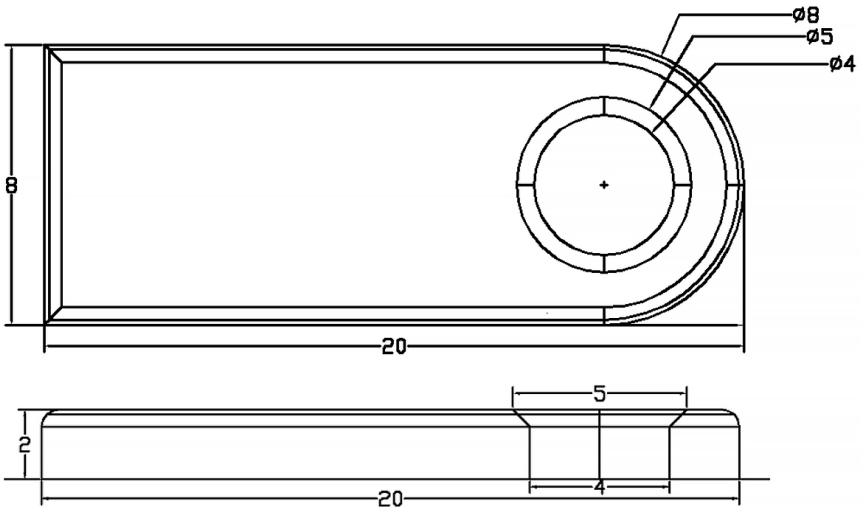

Figure 6. Cranial implant fixture dimension

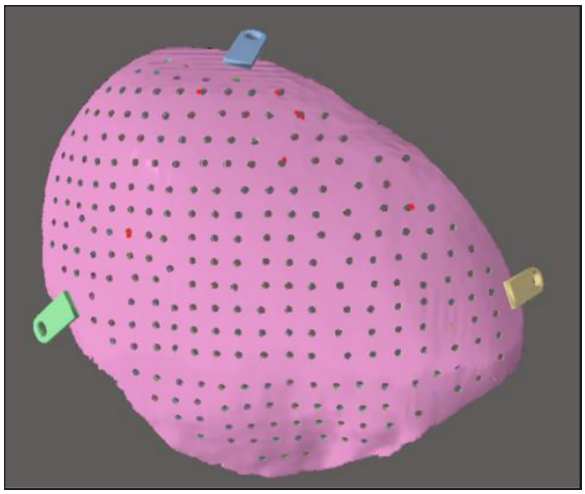

Figure 7. The designed cranial implant with fixture

Manufacture of model prototypes

The additive manufacturing (AM) technique has been used to fabricate the prototypes of the intended models for the defected skull and the designed cranial implant for the patient under study. The AM technology referred to use the additive processes, which combine materials layer by layer. This technique has more benefits, particularly: it is an automated manufacturing process based on layer technology, and it is a freedom fabrication process, so it is able to fabricate any sophisticated geometry of the free form surfaces [14, 15].

The generated models in Figures 5 and 7 were exported as stereolithography (STL) file format to manufacturing software (Ultimaker CURA 4.7) for simulating the manufacturing process using a 3D printing process, as shown in Figure 10. This software enables generating a G-coded tool path for nozzle of a 3D printing machine, also, it can determine the fabrication conditions, such as speed and temperature of printing, the used material and pattern and density of infill. In the present work an Any cubic Mega S 3D printing machine has been used to generate the prototype for the solid model of the skull and implant.

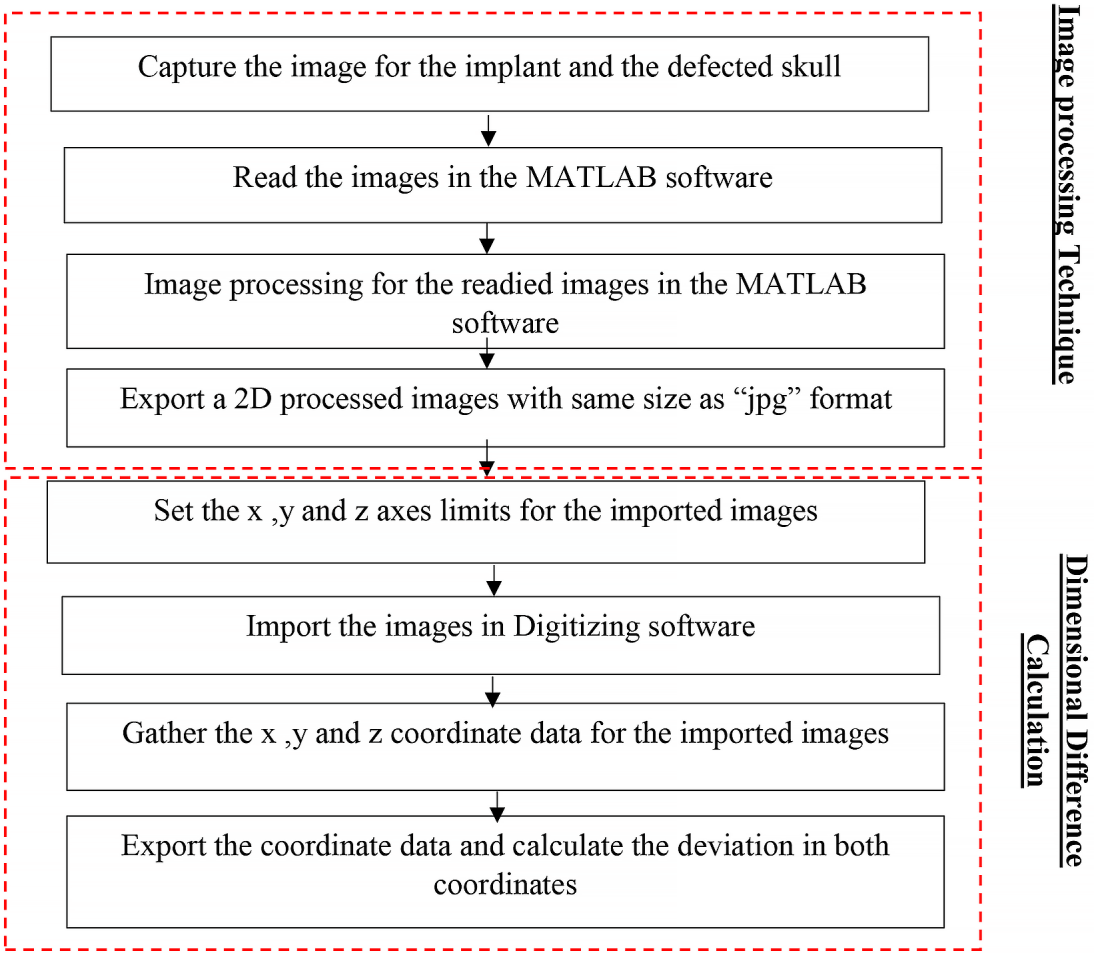

Figure 8. The introduced procedure for image processing and dimensional

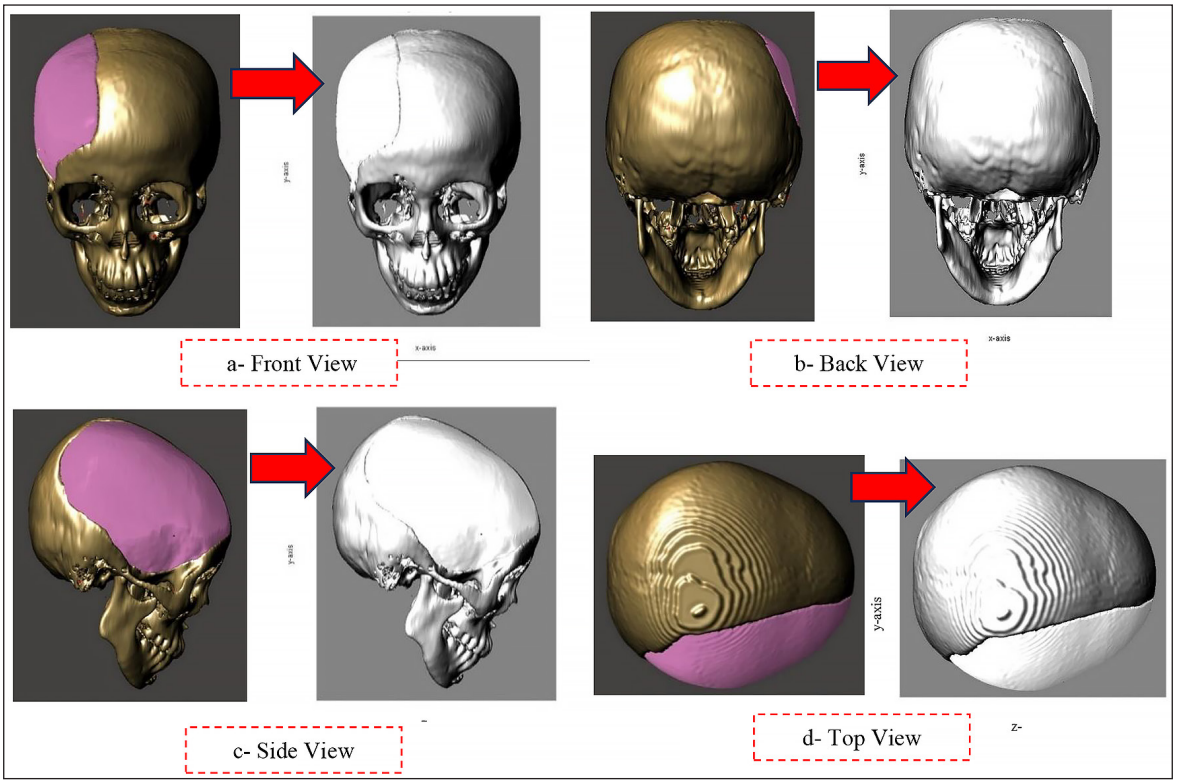

Figure 9. The image processing of the skull and implant image

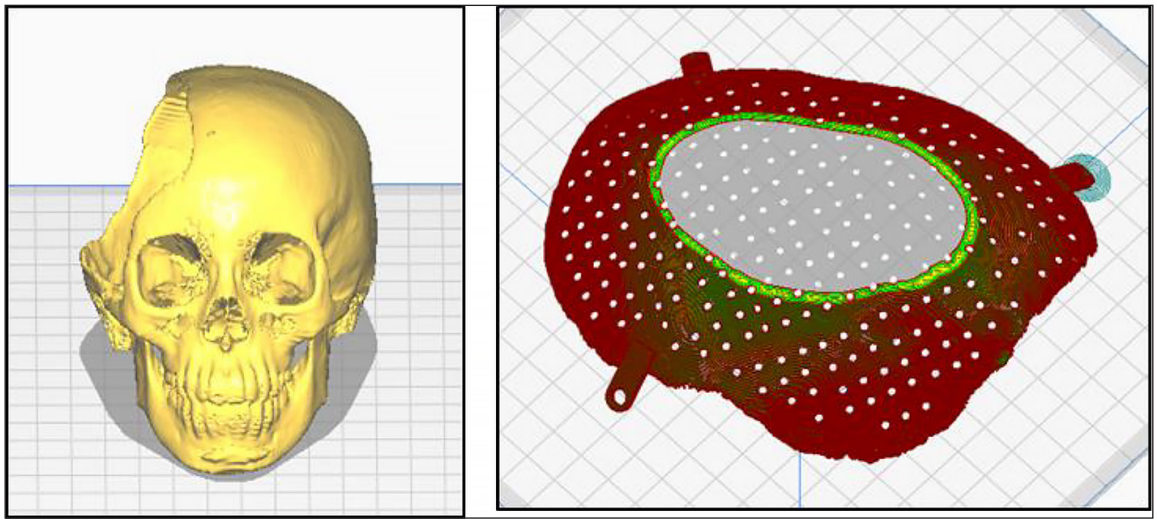

Figure 10. Individual simulation processes for the skull and implant

Polylactic acid (PLA) was used as a filament to generate the 3D physical model of the defected skull and designed implant. The diameter of filament was (1.75 mm), the temperature of printing for nozzle was (200 °C), and the plate temperature sited to (60 °C), also the printing speed was (40 mm/s), while the speed of infill and support were set as (30 mm/s), in addition to 20% infill density with grid pattern.

Figure 11 shows the fabricated prototypes of the defected skull and designed cranial implant using the adopted 3D printer machine.

Dimensional accuracy results

The enhancing procedure that was adopted in the present work was carried out to obtain a precise boundary for the images as a requirement for

Table 1. The digitizing data and difference value for both cranial implant and the defected zone in the skull of the patient with front and back view images

Point no.	View	Skull image		Implant image		The difference value	
		x	y	x	y	x skull-x implant	y skull-y implant
1	Front	110.9146	485.4623	109.0526	484.4918	1.861984	0.970557
2		117.7076	474.4627	117.7076	474.4627	0	0
3		121.5696	460.767	119.6386	460.767	1.630992	0
4		124.4316	443.297	122.5696	443.297	1.861984	0
5		119.6386	427.7681	119.6386	427.7681	0	0
6		119.6386	410.4059	118.7299	410.4059	0.908702	0
7		122.5006	393.0437	120.7386	393.0437	1.761984	0
8		125.4316	369.2111	123.5919	369.2111	1.839694	0
9		124.4316	343.5453	122.6696	342.6826	1.761984	0.862718
10		120.5696	319.8206	119.7299	319.8206	0.839694	0
11		111.0059	299.684	109.9836	301.3505	1.02229	-1.66655
12		97.48896	294.1547	95.75797	295.8507	1.730992	-1.69599
13		78.17904	284.1256	78.17904	284.1256	0	0
14		59.89141	270.3221	58.98271	270.3221	0.908702	0
15		49.32775	257.4892	49.32775	257.4892	0	0
16	Back	264.5143	474.235	264.5143	474.235	0	0
17		280.9805	456.1843	280.9805	456.1843	0	0
18		280.9805	449.9197	281.9555	449.9197	-0.97497	0
19		292.0302	431.869	292.0302	431.869	0	0
20		298.53	415.6233	298.53	416.579	0	-0.95562
21		305.8965	400.3333	307.7381	400.3333	-1.84162	0
22		311.4213	380.4775	313.263	381.4332	-1.84162	-0.95562
23		319.6545	364.2319	320.6294	364.2319	-0.97497	0
24		327.8876	345.3318	327.0209	346.2874	0.86664	-0.95562
25		332.5458	330.0417	332.5458	330.0417	0	0
26		341.7539	311.991	340.7789	311.991	0.97497	0
27		264.5143	474.235	264.5143	474.235	0	0

converting this boundary into coordinate data for these images. Origin pro 2024 software use to digitize the images. Tables 1 and 2 demonstrate the digitizing data and the difference value for horizontal and vertical coordinate for each 2D image dimension, these difference values were calculated for the boundary area of 2D images for the cranial implant and the defected zone in the skull of the patient. Table 1 presents these values for front and back views, while Table 2 shows the dominant value for top and right-side views. The difference values were calculated using the formula in Equation 4.

$$\text{Diff.} = \text{CVDS} - \text{CVCI} \tag{4}$$

where: CVDS – coordinate value of defected skull, CVCI – coordinate value of the cranial implant.

The deviation scattering for the digitized data are shown in Figures 12 and 13 for x and y axis, respectively. The results of the dimensional accuracy are listed in Tables 1 and 2; also, the result of the difference between the edge of skull and the edge of the designed cranial implant for the defected zone in skull are shown as scattering data in Figures 12 and 13.

From these results, it can be noticed that a dimensional deviation value was in the range of ±1.861984 mm, this deviation could be observed due to many reasons, such as, difficulties to detect the boundary of the images during image processing technique, and illumination or orientation problems during capturing images. Despite that, this deviation value was very small, comparing with the dimension of skull and the designed implant.

Table 2. The digitizing data and difference value for both cranial implant and the defected zone in the skull of the patient with top and right-side view images

Point no.	view	Skull image		Implant image		The difference (scattering) value	
		x	y	x	y	x skull-x implant	y skull-y implant
1	Top	87.4242	75.39661	89.22007	75.39661	-1.79587	0
2		92.81181	86.04221	93.76257	84.32863	-0.95076	1.713584
3		100.9461	86.87716	100.9461	86.04221	0	0.834949
4		148.3782	100.2363	149.3289	98.46208	-0.95076	1.774267
5		158.2026	109.0033	159.9985	107.4941	-1.79587	1.509215
6		192.3242	123.1974	192.3242	121.4232	0	1.774267
7		211.128	123.1974	211.128	122.3625	0	0.834949
8		233.5236	127.6853	232.6785	125.911	0.845116	1.774267
9		251.4823	130.0081	251.4823	128.6853	0	1.3228
10		289.935	142.7144	289.935	141.7751	0	0.939318
11		306.0979	147.0979	307.0486	145.3236	-0.95076	1.774267
12		346.4522	155.9692	347.2973	155.9692	-0.84512	0
13		399.2719	170.1633	398.4268	170.1633	0.845116	0
14		525.6167	201.1001	525.6167	199.5516	0	1.548533
15		537.3427	207.4229	536.3919	205.6486	0.950755	1.774267
16	Right-side	137.8849	486.3313	136.9894	486.3313	0.895538	0
17		326.147	361.677	325.6594	362.6416	0.487607	-0.96465
18		326.147	269.8208	325.4554	269.8208	0.691573	0
19		305.0521	250.7422	305.0521	251.5996	0	-0.85747
20		294.1066	243.4537	294.9026	243.4537	-0.79603	0
21		228.2348	217.0866	228.2348	216.1219	0	0.964651
22		218.8814	212.4777	218.8814	212.4777	0	0
23		193.6073	214.2998	193.6073	214.0866	0	0.213231
24		139.5765	281.7182	139.5765	280.7535	0	0.964651
25		104.949	309.9074	104.949	310.7649	0	-0.85747
26		88.03327	322.5551	88.03327	324.3772	0	-1.82212
27		64.35125	368.9655	63.55521	370.4318	0.796034	-1.46635
28		58.4805	385.3645	60.17207	384.5071	-1.69157	0.857467
29		58.78892	412.6963	59.07653	412.6963	-0.28761	0
30		99.87427	473.5765	99.87427	472.719	0	0.857467

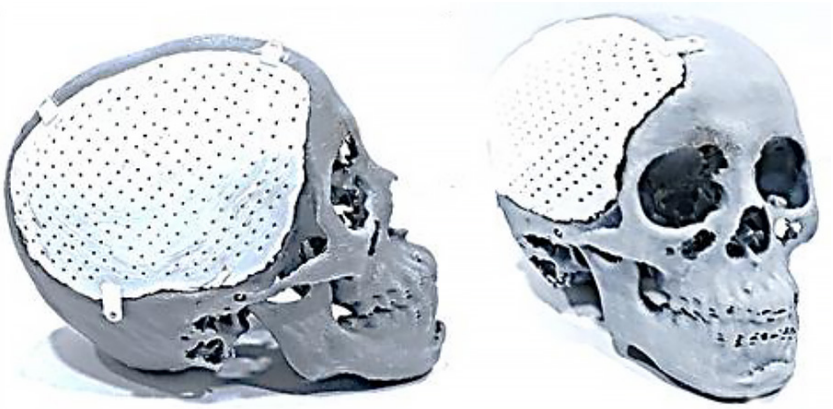

Figure 11. Skull and cranial implant prototypes

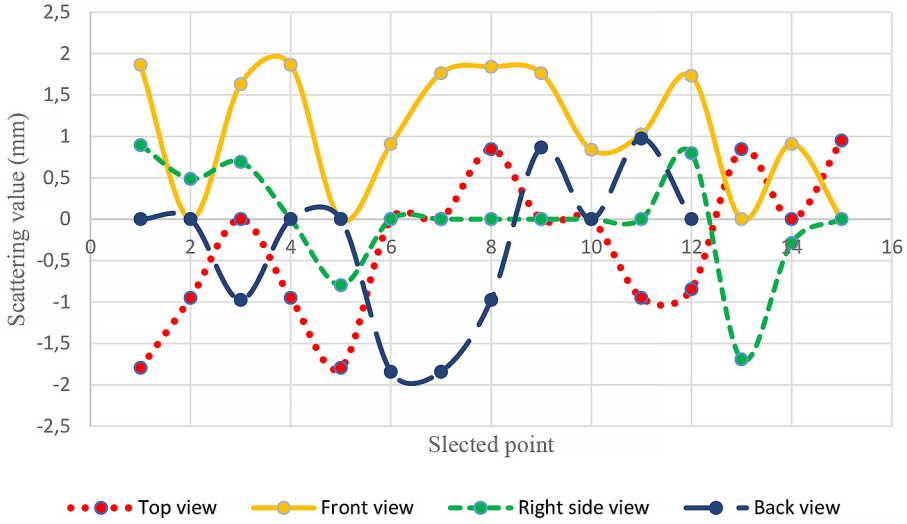

Figure 12. Deviation scattering in x-axis data between skull and implant projection

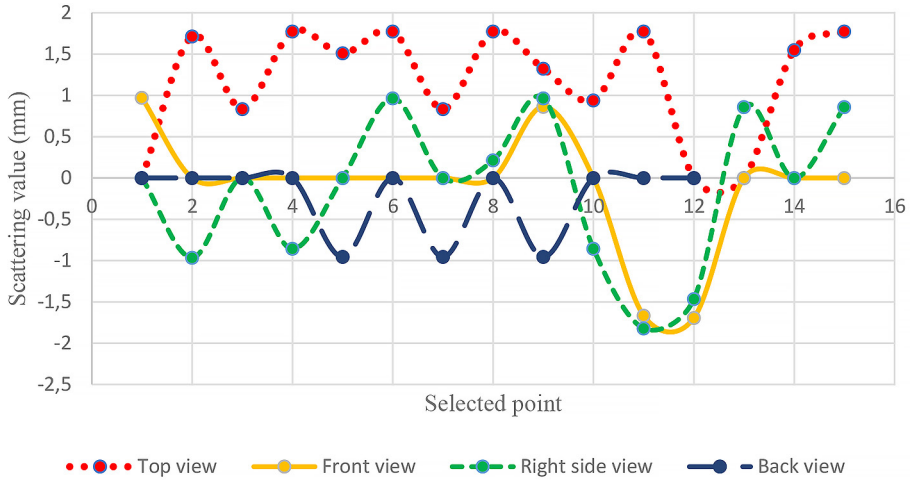

Figure 13. Deviation scattering in y-axis between skull and implant projection

CONCLUSIONS

Utilizing biomedical engineering data in NRRD format collected from CT or MRI scans, specialized algorithms were applied for surface reconstruction through intersection, reflection, and sweeping techniques. The dimensions of the defective skull were (205.7, 149.0, 154.9) mm, while the designed cranial implant measured (139, 131.1, 38.8) mm. MATLAB image processing techniques were employed to calculate the differences between the defective skull and the new implant, yielding a difference range of ±1.861984 mm, which is minimal compared to the overall dimensions of the skull and implant. Fixation components were designed to secure the implant to the skull, allowing for mounting with a 2 mm diameter screw. Additionally, a uniform distribution of circular pores, each with a diameter of 2 mm, was incorporated into the design to reduce the overall weight of the implant. Additive manufacturing technology, specifically 3D printing, was used to create prototypes for both the defective skull and the newly designed cranial implant.

REFERENCES

1. Guvendiren M, Molde J, Soares R, Kohn J. Designing biomaterials for 3D printing. ACS Biomater Sci Eng 2016; 2(10): 1679–1693.
2. Kelly C.N, Miller A.T, Hollister S.J, Guldberg R.E, Gall K. Design and structure–function characterization of 3D printed synthetic porous biomaterials for

tissue engineering. Adv Healthc Mater 2017; 7(7): 1701095.

3. Murphy S.V, Atala A. 3D bioprinting of tissues and organs. Nat Biotechnol 2014; 32(8): 773–785.
4. Dong Ch, Petrovic M, Davies I.J. Applications of 3D printing in medicine: A review. Annals of 3D Printed Medicine, 2024.
5. Boretti A. A perspective on 3D printing in the medical field. Annals of 3D printed medicine, 2024: doi.org/10.1016/j.stlm.2023.100138.
6. Prem Ananth K, Jayram N.D. A comprehensive review of 3D printing techniques for biomaterial-based scaffold fabrication in bone tissue engineering. Annals of 3D printed medicine, 2024.
7. Vindokurov I, Pirogova Y, Tashkinov M, Silberschmidt V.V. Compression of additively manufactured PLA for biomedical applications: Effects of test conditions on properties of solid samples. Polymer Testing, 2024; 130: 108320
8. Zhang M, Qi M.-L, Yuan K, Liu H, Ren J, Liu A, et al. Integrated porous polyetheretherketone implants for treating skull defect. Materials Research and Technology 2023; 22: 728–734.
9. Resmi S, Rimjhim Padam Singh, Kannappan Palaniappan. Automatic skull shape completion of defective skulls using transformers for cranial implant design. International Conference on Machine Learning and Data Engineering (ICMLDE 2023); Procedia Computer Science: 2024; 235: 3305–3314.
10. Nicholas M. Patrikalakis Takashi Maekawa. Shape interrogation for computer aided design and manufacturing. Springer-Verlag Berlin Heidelberg, 2002; doi:10.1007/978-3-642-04074-0.
11. Coleman B. Introduction to Computer Aided Design and Manufacturing. A Jomat Series Training Guide; 2006.
12. Tat McGraw Education Private Limited. CAD CAM Principles and Applications second edition. Tat McGraw Hill Education Pvt.Ltd. 7 West Patal Nagar New Delhi; 2010.
13. Salomon D. Curve and surface for computer graphics. Springer Science and Business Media: USA; 2006.
14. Gebhardt A, Hötter J-S. Additive manufacturing 3D printing for prototyping and manufacturing. Carl Hanser Verlag: Munich; 2016.
15. Gibson I, Rosen D, Stucker B. Additive manufacturing technologies 3D printing, rapid prototyping, and direct digital manufacturing, second edition. Springer Science and Business Media: New York; 2010, 2015.